Sensors and Materials, Vol. 31, No. 12 (2019) 4061–4068
MYU Tokyo

S & M 2069

Method of Estimating Heatstroke Risk Using Wristwatch-type Device

Yoshiyuki Kaiho,[1,2*] Seiichi Takamatsu,[1] and Toshihito Itoh[1]

[1]Department of Human and Engineered Environmental Studies, Graduate School of Frontier Sciences, The University of Tokyo, 5-1-5 Kashiwanoha, Kashiwa-shi, Chiba 277-8563, Japan
[2]Research and Development Center, Corporate Technology Division, Seiko Instruments Inc., 563 Takatsuka-Shinden, Matsudo-shi, Chiba 270-2222, Japan

(Received May 31, 2019; accepted September 10, 2019)

Keywords: heatstroke, WBGT, black globe temperature, neural network, wearable device

As a method of estimating the risk of heatstroke with a wearable device, we have developed a method of calculating the wet bulb globe temperature (WBGT) by estimating the black globe temperature (T_g) only from sensors that can be mounted on a wristwatch-type device. In WBGT measurement, the conventional method requires a large sensor for measuring T_g, and it has been difficult to grasp an individual's heatstroke risk. In this research, we proposed a method of estimating T_g using a neural network and compared the estimation accuracy for different numbers of layers and nodes. In the T_g range of 31 to 41 °C, it was confirmed that when T_g was estimated by the fully connected neural network of three layers and 20 nodes, the regression coefficient between the measured T_g and the estimated T_g was 0.90, indicating a high accuracy.

1. Introduction

In recent years, the number of onsets of heatstroke due to intense summer heat has increased. When an individual has heatstroke, the balance of fluid and salt in the body, as well as the thermoregulatory function, is upset. As a result, the core body temperature rises and causes various symptoms such as dizziness, cramps, and headache.[1,2] The wet bulb globe temperature (WBGT) is an indicator of the external environment related to heatstroke.[3] It is known that the risk of heatstroke increases when WBGT increases and the risk is classified in four categories by the Japanese government. WBGT is calculated from the ambient temperature (T_a), the wet bulb temperature (T_w), and the black globe temperature (T_g). The WBGT outdoors is expressed by

$$WBGT = 0.1 \times T_a + 0.7 \times T_w + 0.2 \times T_g. \quad (1)$$

Among these, T_a is the ambient temperature, and T_w can be calculated from T_a and relative humidity (RH) by using a psychrometric chart.[4] On the other hand, a method of calculating T_g has not been established, and a special sensor is used for its measurement.[5] Therefore, a

*Corresponding author: e-mail: ykaiho@s.h.k.u-tokyo.ac.jp
https://doi.org/10.18494/SAM.2019.2452

ISSN 0914-4935

specially designed sensor has been required for conventional WBGT measurement. Under the present circumstances, WBGT measurement is conducted only at representative points in various locations, and it has been difficult to grasp the heatstroke risk to individuals.

On the other hand, wearable devices have been developed in recent years, and various measurements can be conducted by using wearable devices such as wristwatch-type and glasses-type devices.[6–9] Wearable devices are suitable for monitoring an individual and his/her local surroundings, because a wearable device is used continuously by the same person. Temperature and humidity sensors are conventionally mounted on wristwatch-type devices.[10,11] Therefore, if it is possible to estimate T_g using other sensors applicable to a wearable device, it will be possible to obtain WBGT around that person, which can greatly contribute to the awareness of the individual's heatstroke risk. In the method of obtaining WBGT to assess whether an environment may cause heatstroke, it is possible to take measures to avoid the risk of heatstroke before symptoms occur.

As another way to estimate heatstroke risk, wearable core body temperature sensors have been developed.[12] In this method, a sensor is placed in the ear to measure the eardrum temperature. The method to measure the core body temperature directly is useful for grasping the heatstroke risk. However, since the core body temperature has a small fluctuation range, there may be no time to take appropriate action before the onset of heatstroke symptoms. In addition, it is necessary to insert a sensor into the ear for measurement and cut off it thermally from the outside. In this case, there is a possibility that the ear may be injured in the case of falling or external sounds may not be heard. Although it has been proposed that external sounds can be transmitted by bone conduction, it is necessary to strongly press the device against the body for transmission, which is unsuitable for long-time wearing. However, it is possible to wear a wristwatch-type device for a long time safely without these disadvantages.

Regarding the estimation of T_g, neural networks have attracted attention as a method of estimating a certain state from multiple sensor data.[13,14] A neural network has several intermediate layers between the input layer and the output layer, and each intermediate layer is composed of multiple nodes. As these nodes and layers increase in number, the variety of states that can be estimated becomes richer.[15] However, as the network becomes more complex, computational costs increase and device power consumption increases.[16] In wearable devices, since the power supply is limited, it is necessary to ensure estimation accuracy with a network, that is as simple as possible.

In this research, we compared the estimation accuracy for different numbers of layers and nodes of a neural network to estimate T_g from the data of sensors that can be mounted on a wristwatch-type device.

2. Experimental Methods

2.1 Sensor setup and measurement

In this study, temperature, humidity, illuminance, and skin temperature were selected, because they were considered to be related to T_g and sensors that measure them can be mounted

on a wristwatch-type device. Temperature and humidity are used as information on the state of the outside air, and illuminance is used to reflect information on solar radiation. T_g mainly indicates the effect of radiant heat. Correlated outdoors, radiant heat is dominated by solar radiation, so the measured illuminance is highly associated with solar radiation. In addition, since the skin temperature affects the device as a heat source, the temperature where the human body is in contact with the device is measured. An MR6662 sensor (CHINO Corporation) was used as a temperature and humidity sensor, an HD2102.21 sensor (Delta OHM Corporation) was used as an illuminance sensor, and a TC101A sensor (MadgeTech, Inc.) was used as a skin temperature sensor. As teacher data for performing machine learning, an HI-2000SD WBGT index meter (CUSTOM Corporation) equipped with a T_g sensor was used. The specifications of each sensor are shown in Table 1. In the measurement, each sensor was fixed around the arm and the WBGT index meter was held in the hand as shown in Fig. 1. The measurement was performed outdoors on the premises of the University of Tokyo Kashiwa Campus. The measurement was made once per minute for all sensors. Data was collected several times between 2nd July and 19th September 2018, and a total of 845 min of data was acquired.

Table 1
Specifications of each sensor.

Sensor name	Target	Range	Accuracy
MR6662	Ambient temperature	−30–60 °C	±0.5 °C (−5–50 °C) ±1 °C (−30–−5 °C, 50–60 °C)
	RH	0–100%RH	±3%RH (25 ± 2 °C, 0–90%RH) Temperature coefficient ±0.1%RH/°C (5–60 °C)
HD2102.21	Illuminance	0.01–200 × 103 (lux)	0.01 lux (0.01–199.99 lux) 0.1 lux (–1999.9 lux) 1 lux (–19999 lux) 10 lux (–199.99 × 10^3 lux)
TC101A	Skin temperature	−40–80 °C	0.1 °C
HI-2000SD	Black globe temperature	0–80 °C	±0.6 (15–40 °C)

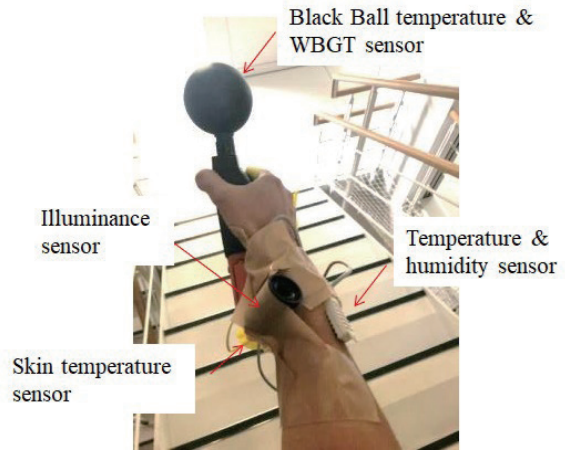

Fig. 1. (Color online) Photograph of sensors placed around an arm.

2.2 Machine learning setup

The measured data were divided into three groups, namely, one for learning and the other two for testing. The first group had 705 min of data. The second group for test 1 and the third group for test 2 had 70 min of data. Learning was performed using 705 sets of data and evaluation was performed using 70 sets of test data, indicating that each set had 1 min of measurement data. To eliminate the bias of the data in each group, all the 845 min of measured data was organized in order of increasing T_g, and the data for the test was created by extracting the data at equal intervals. T_g in all the measured data was distributed in the range shown in Fig. 2.

In this study, the numbers of layers and nodes of the constructed neural network were varied as shown in Table 2, and the estimation accuracy under each condition was evaluated. The activation function between the layers was a rectified linear unit (ReLU) represented by $\varphi(x) = \max(0, x)$. Two evaluation indexes were employed: the regression coefficient between the measured T_g and the estimated T_g, and the standard deviation of the error between the measured T_g and the estimated T_g.

3. Experimental Results

A learning model of a neural network with each parameter was constructed by using learning data, and test data 1 was evaluated. Figure 3 shows the relationship between the measured T_g and the estimated T_g in the cases of 20 nodes and two layers, three layers, and four layers, which are part of the analysis results. The thick black line in each figure represents

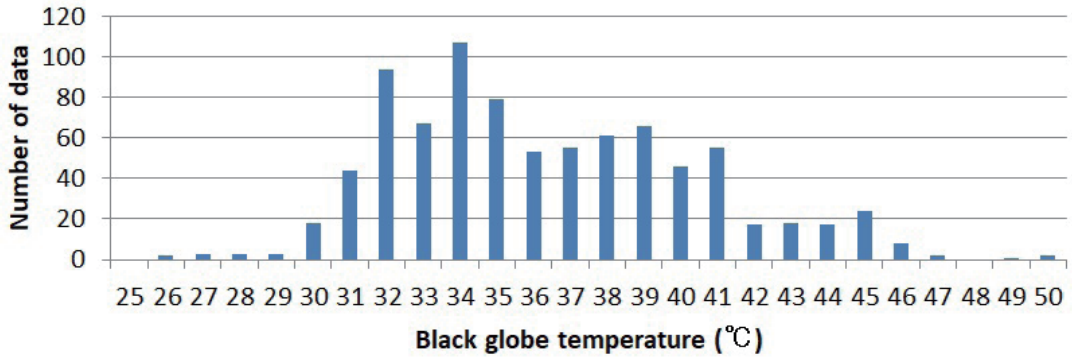

Fig. 2. (Color online) Distribution of measured black globe temperatures.

Table 2
Values of neural network parameters.

Parameter	Values
No. of layers	2, 3, 4
No. of nodes	10, 20, 50, 100, 200

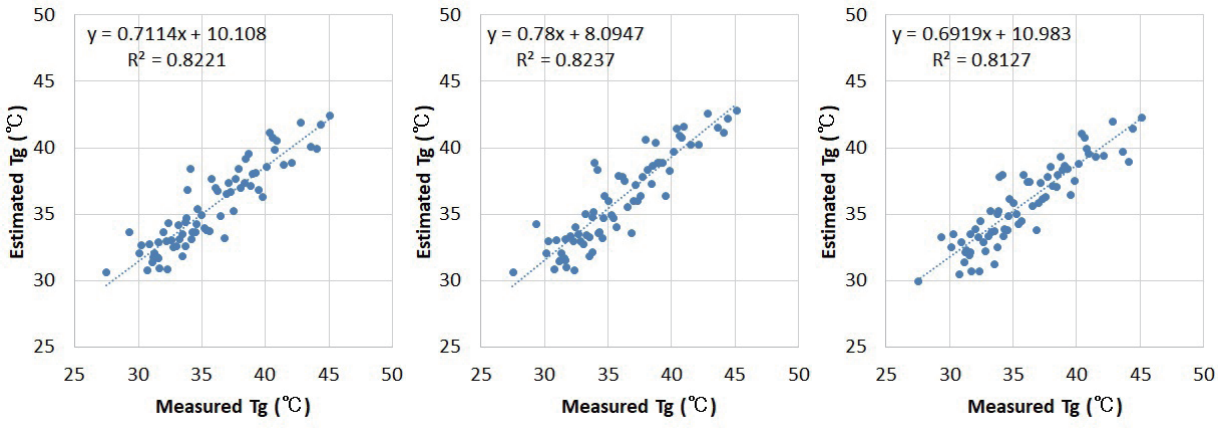

Fig. 3. (Color online) Relationship between measured T_g and estimated T_g in the cases of 20 nodes: (a) two layers, (b) three layers, and (c) four layers.

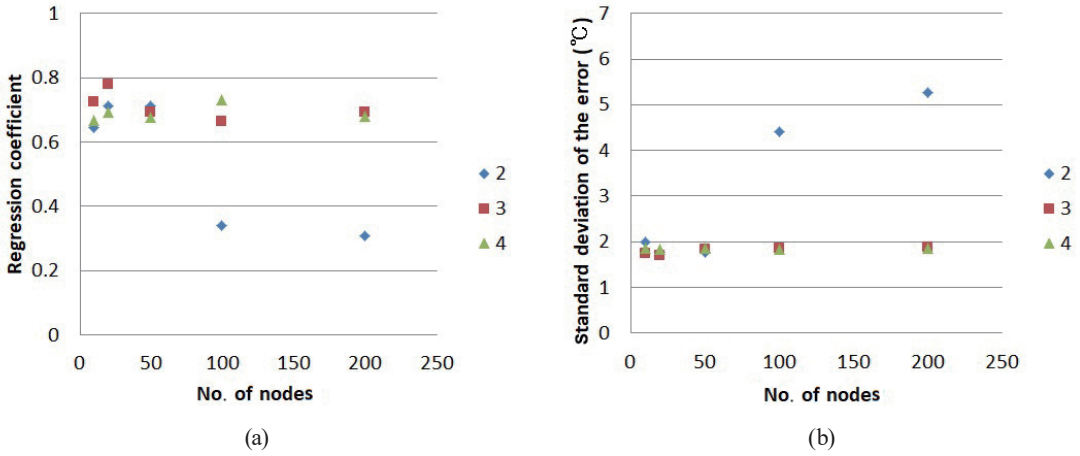

Fig. 4. (Color online) Evaluation results for each pair of neural network parameters: (a) regression coefficient and (b) standard deviation of error.

equal measured and estimated values, that is, a line with a regression coefficient of 1. It was confirmed that the regression coefficient differs in each case. This regression coefficient and the standard deviation of the error between the measured T_g and the estimated T_g are plotted against the number of nodes for each number of layers in Figs. 4(a) and 4(b), respectively. The most desirable result was obtained, with a regression coefficient of 0.78 and a standard deviation of 1.71 °C, in the case above the three layers and 20 nodes. In the case of two layers, a decrease in accuracy was observed above 100 nodes. There was no trend with increasing number of nodes in the case of four layers. From Fig. 4(b), it was confirmed that the deterioration was significant when the number of nodes was more than 100 in the case of two layers.

4. Discussion

From the results, it was confirmed that T_g can be estimated accurately by employing three layers and 20 nodes. In particular, since the accuracy is not improved even if the numbers of layers and nodes are increased, it is considered that three layers and 20 nodes are appropriate for estimating T_g in this system. To confirm the reproducibility of the results, a similar analysis was performed using test data 2. The results are shown in Fig. 5. Despite some errors, the same trend as in test data 1 was obtained, and the highest regression coefficient was obtained for three layers and 20 nodes, thus confirming the reproducibility of the learning model.

Referring to Fig. 3(b), the deviation from the line corresponding to a regression coefficient of 1 is large in the range of T_g of 31.0 °C or lower and 41.0 °C or higher. In the range of 31 to 41 °C, it was found that the regression coefficient was improved to 0.90 as shown in Fig. 6. In the ranges of T_g of 31 °C or lower and 41 °C or higher, the number of acquired data was observed to be as small as about 14% of all the data, as shown in Fig. 2, and it is considered that sufficient learning was not performed.

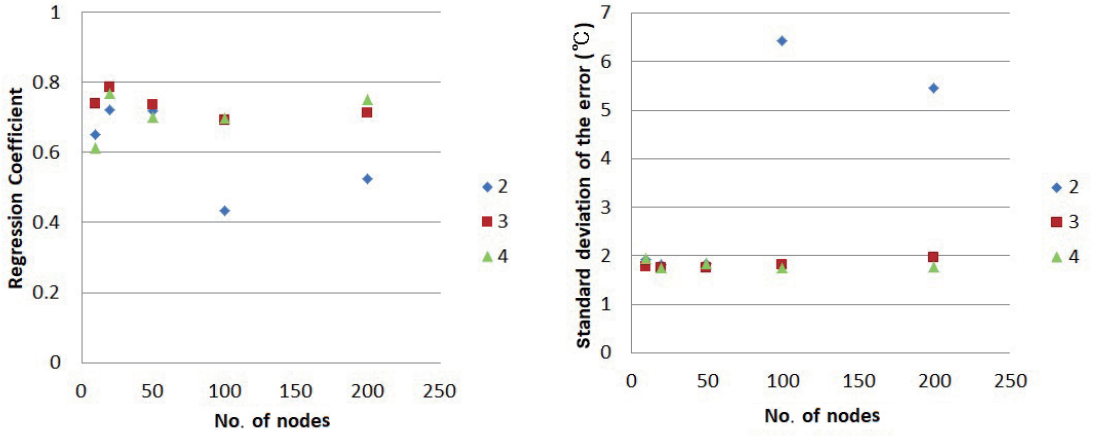

(a) (b)

Fig. 5. (Color online) Evaluation results for each pair of neural network parameters in test data 2: (a) regression coefficient and (b) standard deviation of error.

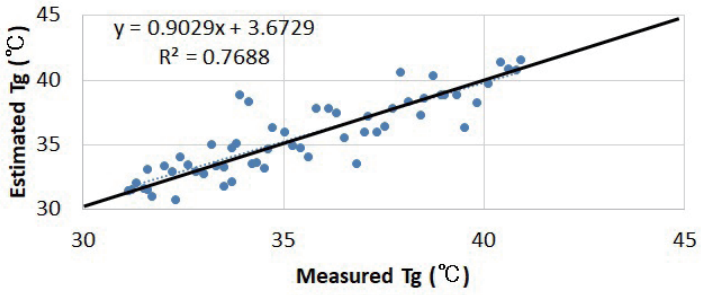

Fig. 6. (Color online) Relationship between the measured T_g and the estimated T_g when T_g is in the range of 31 to 41 °C.

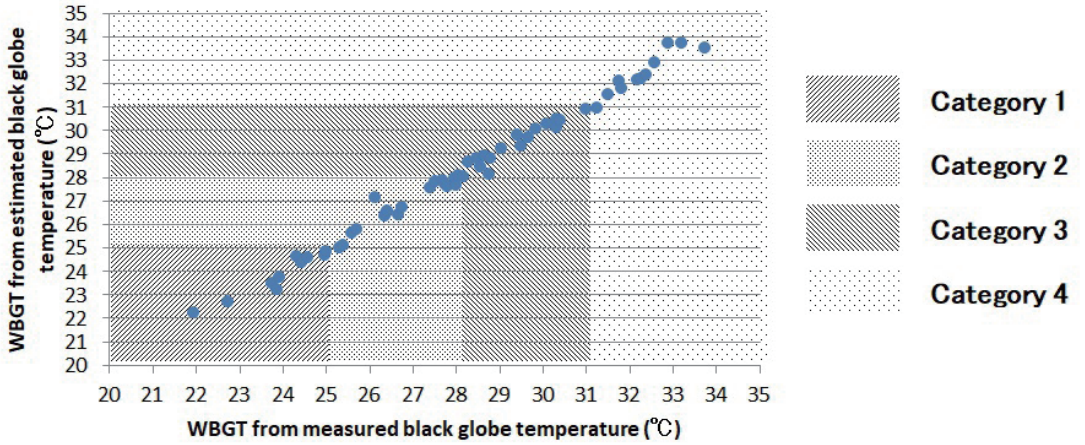

Fig. 7. (Color online) Relationship between WBGT calculated from the measured and estimated T_g values.

To confirm the effect of the estimation accuracy of T_g on the heatstroke risk evaluation, WBGT was calculated using Eq. (1) with the measured and estimated T_g values from test data 1. Figure 7 shows the relationship between WBGT calculated from the measured and estimated T_g values. The maximum error was 1.00 ℃. The multiple areas shown in different patterns are the risk categories defined in Japan.[17] Near the boundary of each risk category, if the WBGT calculated from the estimated T_g is lower than that calculated from the measured T_g, there is a possibility of underestimating the risk when adopting the lower risk category. Therefore, it is possible to prevent the underestimation of the risk by adding 1.00 ℃ to the estimated WBGT, because 1.00 ℃ is the maximum error as described above.

5. Conclusions

In this research, we proposed a method of estimating T_g using a neural network from the data of sensors that can be mounted on a wristwatch-type device, and we compared the estimation accuracy for different numbers of layers and these nodes of the neural network. When T_g was estimated by the three-layer 20-node fully connected neural network, the regression coefficient between the measured T_g and the estimated T_g was 0.78 and the standard deviation of the error was 1.71 ℃, which was the highest accuracy. Similar accuracy was obtained with other test data. In addition, a regression coefficient of 0.90 was obtained when T_g was in the range of 31 to 41 ℃. In the calculation of WBGT using the estimated T_g, the maximum error was 1.00 ℃. It was also found that it is possible to prevent the underestimation of risk by adding 1.00 ℃ to the estimated WBGT.

Acknowledgments

This paper is based on the results obtained from a project commissioned by the New Energy and Industrial Technology Development Organization (NEDO).

References

1 J. L. Glazer: Am. Fam. Physician **1** (2005) 2133. https://www.ncbi.nlm.nih.gov/pubmed/15952443
2 L. R. Leon and A. Bouchama: Compr. Physiol. **5** (2015) 611. https://doi.org/10.1002/cphy.c140017
3 C. P. Yaglou and D. Minaed: Arch. Indust. Health **16** (1957) 302. http://citeseerx.ist.psu.edu/viewdoc/download?doi=10.1.1.501.7943&rep=rep1&type=pdf
4 M. Tahbaz: Int. J. Archit. Eng. Urban. Plan **21** (2011) 95. http://ijaup.iust.ac.ir/browse.php?a_code=A-11-1-29&sid=1&slc_lang=en
5 J. L. Purswell and J. D. Davis: Appl. Eng. Agric. **24** (2008) 379. https://doi.org/10.13031/2013.24500
6 S. C. Mukhopadhyay: IEEE Sens. J. **15** (2014) 1321. https://doi.org/10.1109/JSEN.2014.2370945
7 N. Constant, O. D. Prawl, S. Johnson, and K. Mankodiya: Proc. IEEE 12th Int. Conf. Wearable and Implantable Body Sensor Networks (BSN) (2015). https://doi.org/10.1109/BSN.2015.7299350
8 Y. C. Huang, Y. R. Chen, H. Y. Wu, and Y. J. Huang: Sens. Mater. **31** (2019) 629. https://doi.org/10.18494/SAM.2019.2167
9 H. C. Koydemir and A. Ozcan: Annu. Rev. Anal. Chem. **11** (2018) 127. https://doi.org/10.1146/annurev-anchem-061417-125956
10 T. Klingeberg and M. Schilling: Comput. Meth. Prog. Bio. **106** (2012) 89. https://doi.org/10.1016/j.cmpb.2011.12.009
11 T. Hamatani, A. Uchiyama, and T. Higashino: Proc. IEEE PerCom Workshops (2017). https://doi.org/10.1109/PERCOMW.2017.7917642
12 H. Ota, M. Chao, Y. Gao, E. Wu, L. Tai, K. Chen, Y. Matsuoka, K. Iwai, H. M. Fahad, W. Gao, H. Y. Y. Nyein, L. Lin, and A. Javey: ACS Sens. **2** (2017) 990. https://doi.org/10.1021/acssensors.7b00247
13 A. K. Srivastava: Sens. Actuator B-Chem. **96** (2003) 24. https://doi.org/10.1016/S0925-4005(03)00477-5
14 L. Jing, T. Wang, M. Zhao, and P. Wang: Sensors **17** (2017) 414. https://doi.org/10.3390/s17020414
15 K. He, X. Zhang, S. Ren, and J. Sun: Proc. IEEE Conf. Comput. Vis. Pattern Recognit. (2016) 770. http://openaccess.thecvf.com/content_cvpr_2016/html/He_Deep_Residual_Learning_CVPR_2016_paper.html
16 S. Han, J. Pool, J. Tran, and W. Dally: Proc. 28th Int. Conf. Neural Information Processing Systems (2015) 1135. https://arxiv.org/abs/1506.02626
17 Heatstroke Environmental Health Manual 2018: http://www.wbgt.env.go.jp/pdf/manual/heatillness_manual_full.pdf (in Japanese, accessed July 2019).